Search for the weak radiative decay $\Lambda_c^+ \to \Sigma^+\gamma$ at BESIII

M. Ablikim[1], M. N. Achasov[11,b], P. Adlarson[70], M. Albrecht[4], R. Aliberti[31], A. Amoroso[69A,69C], M. R. An[35], Q. An[66,53], X. H. Bai[61], Y. Bai[52], O. Bakina[32], R. Baldini Ferroli[26A], I. Balossino[27A], Y. Ban[42,g], V. Batozskaya[1,40], D. Becker[31], K. Begzsuren[29], N. Berger[31], M. Bertani[26A], D. Bettoni[27A], F. Bianchi[69A,69C], J. Bloms[63], A. Bortone[69A,69C], I. Boyko[32], R. A. Briere[5], A. Brueggemann[63], H. Cai[71], X. Cai[1,53], A. Calcaterra[26A], G. F. Cao[1,58], N. Cao[1,58], S. A. Cetin[57A], J. F. Chang[1,53], W. L. Chang[1,58], G. Chelkov[32,a], C. Chen[39], Chao Chen[50], G. Chen[1], H. S. Chen[1,58], M. L. Chen[1,53], S. J. Chen[38], S. M. Chen[56], T. Chen[1,58], X. R. Chen[28,58], X. T. Chen[1,58], Y. B. Chen[1,53], Z. J. Chen[23,h], W. S. Cheng[69C], S. K. Choi [50], X. Chu[39], G. Cibinetto[27A], F. Cossio[69C], J. J. Cui[45], H. L. Dai[1,53], J. P. Dai[73], A. Dbeyssi[17], R. E. de Boer[4], D. Dedovich[32], Z. Y. Deng[1], A. Denig[31], I. Denysenko[32], M. Destefanis[69A,69C], F. De Mori[69A,69C], Y. Ding[36], J. Dong[1,53], L. Y. Dong[1,58], M. Y. Dong[1,53,58], X. Dong[71], S. X. Du[75], P. Egorov[32,a], Y. L. Fan[71], J. Fang[1,53], S. S. Fang[1,58], W. X. Fang[1], Y. Fang[1], R. Farinelli[27A], L. Fava[69B,69C], F. Feldbauer[4], G. Felici[26A], C. Q. Feng[66,53], J. H. Feng[54], K Fischer[64], M. Fritsch[4], C. Fritzsch[63], C. D. Fu[1], H. Gao[58], Y. N. Gao[42,g], Yang Gao[66,53], S. Garbolino[69C], I. Garzia[27A,27B], P. T. Ge[71], Z. W. Ge[38], C. Geng[54], E. M. Gersabeck[62], A Gilman[64], K. Goetzen[12], L. Gong[36], W. X. Gong[1,53], W. Gradl[31], M. Greco[69A,69C], L. M. Gu[38], M. H. Gu[1,53], Y. T. Gu[14], C. Y. Guan[1,58], A. Q. Guo[28,58], L. B. Guo[37], R. P. Guo[44], Y. P. Guo[10,f], A. Guskov[32,a], T. T. Han[45], W. Y. Han[35], X. Q. Hao[18], F. A. Harris[60], K. K. He[50], K. L. He[1,58], F. H. Heinsius[4], C. H. Heinz[31], Y. K. Heng[1,53,58], C. Herold[55], G. Y. Hou[1,58], Y. R. Hou[58], Z. L. Hou[1], H. M. Hu[1,58], J. F. Hu[51,i], T. Hu[1,53,58], Y. Hu[1], G. S. Huang[66,53], K. X. Huang[54], L. Q. Huang[28,58], X. T. Huang[45], Y. P. Huang[1], Z. Huang[42,g], T. Hussain[68], N Hüsken[25,31], W. Imoehl[25], M. Irshad[66,53], J. Jackson[25], S. Jaeger[4], S. Janchiv[29], E. Jang[50], J. H. Jeong[50], Q. Ji[1], Q. P. Ji[18], X. B. Ji[1,58], X. L. Ji[1,53], Y. Y. Ji[45], Z. K. Jia[66,53], H. B. Jiang[45], S. S. Jiang[35], X. S. Jiang[1,53,58], Y. Jiang[58], J. B. Jiao[45], Z. Jiao[21], S. Jin[38], Y. Jin[61], M. Q. Jing[1,58], T. Johansson[70], N. Kalantar-Nayestanaki[59], X. S. Kang[36], R. Kappert[59], M. Kavatsyuk[59], B. C. Ke[75], I. K. Keshk[4], A. Khoukaz[63], R. Kiuchi[1], R. Kliemt[12], L. Koch[33], O. B. Kolcu[57A], B. Kopf[4], M. Kuemmel[4], M. Kuessner[4], A. Kupsc[40,70], W. Kühn[33], J. J. Lane[62], J. S. Lange[33], P. Larin[17], A. Lavania[24], L. Lavezzi[69A,69C], T. T. Lei[66,k], Z. H. Lei[66,53], H. Leithoff[31], M. Lellmann[31], T. Lenz[31], C. Li[43], C. Li[39], C. H. Li[35], Cheng Li[66,53], D. M. Li[75], F. Li[1,53], G. Li[1], H. Li[47], H. Li[66,53], H. B. Li[1,58], H. J. Li[18], H. N. Li[51,i], J. Q. Li[4], J. S. Li[54], J. W. Li[45], Ke Li[1], L. J Li[1,58], L. K. Li[1], Lei Li[3], M. H. Li[39], P. R. Li[34,j,k], S. X. Li[10], S. Y. Li[56], T. Li[45], W. D. Li[1,58], W. G. Li[1], X. H. Li[66,53], X. L. Li[45], Xiaoyu Li[1,58], Y. G. Li[42,g], Z. X. Li[14], Z. Y. Li[54], H. Liang[1,58], H. Liang[30], H. Liang[66,53], Y. F. Liang[49], Y. T. Liang[28,58], G. R. Liao[13], L. Z. Liao[45], J. Libby[24], A. Limphirat[55], C. X. Lin[54], D. X. Lin[28,58], T. Lin[1], B. J. Liu[1], C. X. Liu[1], D. Liu[17,66], F. H. Liu[48], Fang Liu[1], Feng Liu[6], G. M. Liu[51,i], H. Liu[34,j,k], H. B. Liu[14], H. M. Liu[1,58], Huanhuan Liu[1], Huihui Liu[19], J. B. Liu[66,53], J. L. Liu[67], J. Y. Liu[1,58], K. Liu[1], K. Y. Liu[36], Ke Liu[20], L. Liu[66,53], Lu Liu[39], M. H. Liu[10,f], P. L. Liu[1], Q. Liu[58], S. B. Liu[66,53], T. Liu[10,f], W. K. Liu[39], W. M. Liu[66,53], X. Liu[34,j,k], Y. Liu[34,j,k], Y. B. Liu[39], Z. A. Liu[1,53,58], Z. Q. Liu[45], X. C. Lou[1,53,58], F. X. Lu[54], H. J. Lu[21], J. G. Lu[1,53], X. L. Lu[1], Y. Lu[7], Y. P. Lu[1,53], Z. H. Lu[1,58], C. L. Luo[37], M. X. Luo[74], T. Luo[10,f], X. L. Luo[1,53], X. R. Lyu[58], Y. F. Lyu[39], F. C. Ma[36], H. L. Ma[1], L. L. Ma[45], M. M. Ma[1,58], Q. M. Ma[1], R. Q. Ma[1,58], R. T. Ma[58], X. Y. Ma[1,53], Y. Ma[42,g], F. E. Maas[17], M. Maggiora[69A,69C], S. Maldaner[4], S. Malde[64], Q. A. Malik[68], A. Mangoni[26B], Y. J. Mao[42,g], Z. P. Mao[1], S. Marcello[69A,69C], Z. X. Meng[61], J. G. Messchendorp[12,59], G. Mezzadri[27A], H. Miao[1,58], T. J. Min[38], R. E. Mitchell[25], X. H. Mo[1,53,58], N. Yu. Muchnoi[11,b], Y. Nefedov[32], F. Nerling[17,d], I. B. Nikolaev[11,b], Z. Ning[1,53], S. Nisar[9,l], Y. Niu [45], S. L. Olsen[58], Q. Ouyang[1,53,58], S. Pacetti[26B,26C], X. Pan[10,f], Y. Pan[52], A. Pathak[30], Y. P. Pei[66,53], M. Pelizaeus[4], H. P. Peng[66,53], K. Peters[12,d], J. L. Ping[37], R. G. Ping[1,58], S. Plura[31], S. Pogodin[32], V. Prasad[66,53], F. Z. Qi[1], H. Qi[66,53], H. R. Qi[56], M. Qi[38], T. Y. Qi[10,f], S. Qian[1,53], W. B. Qian[58], Z. Qian[54], C. F. Qiao[58], J. J. Qin[67], L. Q. Qin[13], X. P. Qin[10,f], X. S. Qin[45], Z. H. Qin[1,53], J. F. Qiu[1], S. Q. Qu[56], K. H. Rashid[68], C. F. Redmer[31], K. J. Ren[35], A. Rivetti[69C], V. Rodin[59], M. Rolo[69C], G. Rong[1,58], Ch. Rosner[17], S. N. Ruan[39], A. Sarantsev[32,c], Y. Schelhaas[31], C. Schnier[4], K. Schoenning[70], M. Scodeggio[27A,27B], K. Y. Shan[10,f], W. Shan[22], X. Y. Shan[66,53], J. F. Shangguan[50], L. G. Shao[1,58], M. Shao[66,53], C. P. Shen[10,f], H. F. Shen[1,58], X. Y. Shen[1,58], B. A. Shi[58], H. C. Shi[66,53], J. Y. Shi[1], Q. Q. Shi[50], R. S. Shi[1,58], X. Shi[1,53], X. D Shi[66,53], J. J. Song[18], W. M. Song[30,1], Y. X. Song[42,g], S. Sosio[69A,69C], S. Spataro[69A,69C], F. Stieler[31], K. X. Su[71], P. P. Su[50], Y. J. Su[58], G. X. Sun[1], H. Sun[58], H. K. Sun[1], J. F. Sun[18], L. Sun[71], S. S. Sun[1,58], T. Sun[1,58], W. Y. Sun[30], X Sun[23,h], Y. J. Sun[66,53], Y. Z. Sun[1], Z. T. Sun[45], Y. H. Tan[71], Y. X. Tan[66,53], C. J. Tang[49], G. Y. Tang[1], J. Tang[54], L. Y Tao[67], Q. T. Tao[23,h], M. Tat[64], J. X. Teng[66,53], V. Thoren[70], W. H. Tian[47], Y. Tian[28,58], I. Uman[57B], B. Wang[66,53], B. Wang[1], B. L. Wang[58], C. W. Wang[38], D. Y. Wang[42,g], F. Wang[67], H. J. Wang[34,j,k], H. P. Wang[1,58], K. Wang[1,53], L. L. Wang[1], M. Wang[45], M. Z. Wang[42,g], Meng Wang[1,58], S. Wang[13], S. Wang[10,f], T. Wang[10,f],

T. J. Wang[39], W. Wang[54], W. H. Wang[71], W. P. Wang[66,53], X. Wang[42,g], X. F. Wang[34,j,k], X. L. Wang[10,f],
Y. Wang[56], Y. D. Wang[41], Y. F. Wang[1,53,58], Y. H. Wang[43], Y. Q. Wang[1], Yaqian Wang[16,1], Z. Wang[1,53],
Z. Y. Wang[1,58], Ziyi Wang[58], D. H. Wei[13], F. Weidner[63], S. P. Wen[1], D. J. White[62], U. Wiedner[4], G. Wilkinson[64],
M. Wolke[70], L. Wollenberg[4], J. F. Wu[1,58], L. H. Wu[1], L. J. Wu[1,58], X. Wu[10,f], X. H. Wu[30], Y. Wu[66], Y. J Wu[28],
Z. Wu[1,53], L. Xia[66,53], T. Xiang[42,g], D. Xiao[34,j,k], G. Y. Xiao[38], H. Xiao[10,f], S. Y. Xiao[1], Y. L. Xiao[10,f],
Z. J. Xiao[37], C. Xie[38], X. H. Xie[42,g], Y. Xie[45], Y. G. Xie[1,53], Y. H. Xie[6], Z. P. Xie[66,53], T. Y. Xing[1,58], C. F. Xu[1,58],
C. J. Xu[54], G. F. Xu[1], H. Y. Xu[61], Q. J. Xu[15], X. P. Xu[50], Y. C. Xu[58], Z. P. Xu[38], F. Yan[10,f], L. Yan[10,f],
W. B. Yan[66,53], W. C. Yan[75], H. J. Yang[46,e], H. L. Yang[30], H. X. Yang[1], L. Yang[47], S. L. Yang[58], Tao Yang[1],
Y. F. Yang[39], Y. X. Yang[1,58], Yifan Yang[1,58], M. Ye[1,53], M. H. Ye[8], J. H. Yin[1], Z. Y. You[54], B. X. Yu[1,53,58],
C. X. Yu[39], G. Yu[1,58], T. Yu[67], X. D. Yu[42,g], C. Z. Yuan[1,58], L. Yuan[2], S. C. Yuan[1], X. Q. Yuan[1], Y. Yuan[1,58],
Z. Y. Yuan[54], C. X. Yue[35], A. A. Zafar[68], F. R. Zeng[45], X. Zeng[6], Y. Zeng[23,h], Y. H. Zhan[54], A. Q. Zhang[1,58],
B. L. Zhang[1,58], B. X. Zhang[1], D. H. Zhang[39], G. Y. Zhang[18], H. Zhang[66], H. H. Zhang[30], H. H. Zhang[54],
H. Y. Zhang[1,53], J. L. Zhang[72], J. Q. Zhang[37], J. W. Zhang[1,53,58], J. X. Zhang[34,j,k], J. Y. Zhang[1], J. Z. Zhang[1,58],
Jianyu Zhang[1,58], Jiawei Zhang[1,58], L. M. Zhang[56], L. Q. Zhang[54], Lei Zhang[38], P. Zhang[1], Q. Y. Zhang[35,75],
Shuihan Zhang[1,58], Shulei Zhang[23,h], X. D. Zhang[41], X. M. Zhang[1], X. Y. Zhang[45], X. Y. Zhang[50], Y. Zhang[64], Y.
T. Zhang[75], Y. H. Zhang[1,53], Yan Zhang[66,53], Yao Zhang[1], Z. H. Zhang[1], Z. Y. Zhang[71], Z. Y. Zhang[39],
G. Zhao[1], J. Zhao[35], J. Y. Zhao[1,58], J. Z. Zhao[1,53], Lei Zhao[66,53], Ling Zhao[1], M. G. Zhao[39], Q. Zhao[1],
S. J. Zhao[75], Y. B. Zhao[1,53], Y. X. Zhao[28,58], Z. G. Zhao[66,53], A. Zhemchugov[32,a], B. Zheng[67], J. P. Zheng[1,53],
Y. H. Zheng[58], B. Zhong[37], C. Zhong[67], X. Zhong[54], H. Zhou[45], L. P. Zhou[1,58], X. Zhou[71], X. K. Zhou[58],
X. R. Zhou[66,53], X. Y. Zhou[35], Y. Z. Zhou[10,f], J. Zhu[39], K. Zhu[1], K. J. Zhu[1,53,58], L. X. Zhu[58], S. H. Zhu[65],
S. Q. Zhu[38], T. J. Zhu[72], W. J. Zhu[10,f], Y. C. Zhu[66,53], Z. A. Zhu[1,58], B. S. Zou[1], J. H. Zou[1], J. Zu[66,53]

(BESIII Collaboration)

[1] Institute of High Energy Physics, Beijing 100049, People's Republic of China
[2] Beihang University, Beijing 100191, People's Republic of China
[3] Beijing Institute of Petrochemical Technology, Beijing 102617, People's Republic of China
[4] Bochum Ruhr-University, D-44780 Bochum, Germany
[5] Carnegie Mellon University, Pittsburgh, Pennsylvania 15213, USA
[6] Central China Normal University, Wuhan 430079, People's Republic of China
[7] Central South University, Changsha 410083, People's Republic of China
[8] China Center of Advanced Science and Technology, Beijing 100190, People's Republic of China
[9] COMSATS University Islamabad, Lahore Campus, Defence Road, Off Raiwind Road, 54000 Lahore, Pakistan
[10] Fudan University, Shanghai 200433, People's Republic of China
[11] G.I. Budker Institute of Nuclear Physics SB RAS (BINP), Novosibirsk 630090, Russia
[12] GSI Helmholtzcentre for Heavy Ion Research GmbH, D-64291 Darmstadt, Germany
[13] Guangxi Normal University, Guilin 541004, People's Republic of China
[14] Guangxi University, Nanning 530004, People's Republic of China
[15] Hangzhou Normal University, Hangzhou 310036, People's Republic of China
[16] Hebei University, Baoding 071002, People's Republic of China
[17] Helmholtz Institute Mainz, Staudinger Weg 18, D-55099 Mainz, Germany
[18] Henan Normal University, Xinxiang 453007, People's Republic of China
[19] Henan University of Science and Technology, Luoyang 471003, People's Republic of China
[20] Henan University of Technology, Zhengzhou 450001, People's Republic of China
[21] Huangshan College, Huangshan 245000, People's Republic of China
[22] Hunan Normal University, Changsha 410081, People's Republic of China
[23] Hunan University, Changsha 410082, People's Republic of China
[24] Indian Institute of Technology Madras, Chennai 600036, India
[25] Indiana University, Bloomington, Indiana 47405, USA
[26] INFN Laboratori Nazionali di Frascati , (A)INFN Laboratori Nazionali di Frascati, I-00044, Frascati, Italy;
(B)INFN Sezione di Perugia, I-06100, Perugia, Italy; (C)University of Perugia, I-06100, Perugia, Italy
[27] INFN Sezione di Ferrara, (A)INFN Sezione di Ferrara, I-44122,
Ferrara, Italy; (B)University of Ferrara, I-44122, Ferrara, Italy
[28] Institute of Modern Physics, Lanzhou 730000, People's Republic of China
[29] Institute of Physics and Technology, Peace Avenue 54B, Ulaanbaatar 13330, Mongolia

[30] *Jilin University, Changchun 130012, People's Republic of China*

[31] *Johannes Gutenberg University of Mainz, Johann-Joachim-Becher-Weg 45, D-55099 Mainz, Germany*

[32] *Joint Institute for Nuclear Research, 141980 Dubna, Moscow region, Russia*

[33] *Justus-Liebig-Universitaet Giessen, II. Physikalisches Institut, Heinrich-Buff-Ring 16, D-35392 Giessen, Germany*

[34] *Lanzhou University, Lanzhou 730000, People's Republic of China*

[35] *Liaoning Normal University, Dalian 116029, People's Republic of China*

[36] *Liaoning University, Shenyang 110036, People's Republic of China*

[37] *Nanjing Normal University, Nanjing 210023, People's Republic of China*

[38] *Nanjing University, Nanjing 210093, People's Republic of China*

[39] *Nankai University, Tianjin 300071, People's Republic of China*

[40] *National Centre for Nuclear Research, Warsaw 02-093, Poland*

[41] *North China Electric Power University, Beijing 102206, People's Republic of China*

[42] *Peking University, Beijing 100871, People's Republic of China*

[43] *Qufu Normal University, Qufu 273165, People's Republic of China*

[44] *Shandong Normal University, Jinan 250014, People's Republic of China*

[45] *Shandong University, Jinan 250100, People's Republic of China*

[46] *Shanghai Jiao Tong University, Shanghai 200240, People's Republic of China*

[47] *Shanxi Normal University, Linfen 041004, People's Republic of China*

[48] *Shanxi University, Taiyuan 030006, People's Republic of China*

[49] *Sichuan University, Chengdu 610064, People's Republic of China*

[50] *Soochow University, Suzhou 215006, People's Republic of China*

[51] *South China Normal University, Guangzhou 510006, People's Republic of China*

[52] *Southeast University, Nanjing 211100, People's Republic of China*

[53] *State Key Laboratory of Particle Detection and Electronics, Beijing 100049, Hefei 230026, People's Republic of China*

[54] *Sun Yat-Sen University, Guangzhou 510275, People's Republic of China*

[55] *Suranaree University of Technology, University Avenue 111, Nakhon Ratchasima 30000, Thailand*

[56] *Tsinghua University, Beijing 100084, People's Republic of China*

[57] *Turkish Accelerator Center Particle Factory Group, (A)Istinye University, 34010, Istanbul, Turkey; (B)Near East University, Nicosia, North Cyprus, Mersin 10, Turkey*

[58] *University of Chinese Academy of Sciences, Beijing 100049, People's Republic of China*

[59] *University of Groningen, NL-9747 AA Groningen, The Netherlands*

[60] *University of Hawaii, Honolulu, Hawaii 96822, USA*

[61] *University of Jinan, Jinan 250022, People's Republic of China*

[62] *University of Manchester, Oxford Road, Manchester, M13 9PL, United Kingdom*

[63] *University of Muenster, Wilhelm-Klemm-Strasse 9, 48149 Muenster, Germany*

[64] *University of Oxford, Keble Road, Oxford OX13RH, United Kingdom*

[65] *University of Science and Technology Liaoning, Anshan 114051, People's Republic of China*

[66] *University of Science and Technology of China, Hefei 230026, People's Republic of China*

[67] *University of South China, Hengyang 421001, People's Republic of China*

[68] *University of the Punjab, Lahore-54590, Pakistan*

[69] *University of Turin and INFN, (A)University of Turin, I-10125, Turin, Italy; (B)University of Eastern Piedmont, I-15121, Alessandria, Italy; (C)INFN, I-10125, Turin, Italy*

[70] *Uppsala University, Box 516, SE-75120 Uppsala, Sweden*

[71] *Wuhan University, Wuhan 430072, People's Republic of China*

[72] *Xinyang Normal University, Xinyang 464000, People's Republic of China*

[73] *Yunnan University, Kunming 650500, People's Republic of China*

[74] *Zhejiang University, Hangzhou 310027, People's Republic of China*

[75] *Zhengzhou University, Zhengzhou 450001, People's Republic of China*

[a] *Also at the Moscow Institute of Physics and Technology, Moscow 141700, Russia*

[b] *Also at the Novosibirsk State University, Novosibirsk, 630090, Russia*

[c] *Also at the NRC "Kurchatov Institute", PNPI, 188300, Gatchina, Russia*

[d] *Also at Goethe University Frankfurt, 60323 Frankfurt am Main, Germany*

[e] Also at Key Laboratory for Particle Physics, Astrophysics and Cosmology, Ministry
of Education; Shanghai Key Laboratory for Particle Physics and Cosmology; Institute
of Nuclear and Particle Physics, Shanghai 200240, People's Republic of China

[f] Also at Key Laboratory of Nuclear Physics and Ion-beam Application (MOE) and Institute
of Modern Physics, Fudan University, Shanghai 200443, People's Republic of China

[g] Also at State Key Laboratory of Nuclear Physics and Technology,
Peking University, Beijing 100871, People's Republic of China

[h] Also at School of Physics and Electronics, Hunan University, Changsha 410082, China

[i] Also at Guangdong Provincial Key Laboratory of Nuclear Science, Institute of
Quantum Matter, South China Normal University, Guangzhou 510006, China

[j] Also at Frontiers Science Center for Rare Isotopes, Lanzhou University, Lanzhou 730000, People's Republic of China

[k] Also at Lanzhou Center for Theoretical Physics, Lanzhou University, Lanzhou 730000, People's Republic of China

[l] Also at the Department of Mathematical Sciences, IBA, Karachi , Pakistan

The Cabibbo-allowed weak radiative decay $\Lambda_c^+ \to \Sigma^+\gamma$ has been searched for in a sample of $\Lambda_c^+\bar{\Lambda}_c^-$ pairs produced in e^+e^- annihilations, corresponding to an integrated luminosity of 4.5 fb^{-1} collected with the BESIII detector at center-of-mass energies between 4.60 and 4.70 GeV. No excess of signal above background is observed, and we set an upper limit on the branching fraction of this decay to be $\mathcal{B}(\Lambda_c^+ \to \Sigma^+\gamma) < 4.4 \times 10^{-4}$ at a confidence level of 90%, which is in agreement with Standard Model expectations.

I. INTRODUCTION

Charmed baryons provide an excellent laboratory for studying the dynamics of light quarks in the environment of a heavy quark [1, 2]. However, to date, there is no satisfactory phenomenological approach for describing the complicated physics of charmed-baryon decays. Improved experimental results are essential for us to understand better the underlying physics and constrain the relevant models. In recent years, great progress has been made in the experimental study of the Λ_c^+ baryon at the BESIII, Belle and LHCb experiments, including precise measurements of the $e^+e^- \to \Lambda_c^+\bar{\Lambda}_c^-$ production cross sections [3], the branching fractions (BFs) of Cabibbo-favored and suppressed hadronic decays [4, 5], the BFs of semi-leptonic decays [6, 7] and of hadronic weak decays [8], as well as searches for very rare processes [9]. Thanks to a large $\Lambda_c^+\bar{\Lambda}_c^-$ data sample, corresponding to an integrated luminosity of 4.5 fb^{-1}, BF studies at BESIII have the potential to reach a sensitivity of 10^{-4}, which is sufficient to search for unmeasured Λ_c^+ decays with low BFs and perform precise measurements of the BFs of known Λ_c^+ decays. For example, with this sample BESIII has reported the first observation of the Cabibbo-suppressed decay $\Lambda_c^+ \to n\pi^+$ with a BF of $(6.6\pm1.3)\times10^{-4}$ [10]. Throughout this paper, the charge conjugated decay channels are implied.

Radiative decays of charmed hadrons play an important role in understanding their dynamics. Weak radiative decays usually receive contributions from both the weak and electromagnetic interactions. In addition, long-distance effects could be comparable to, or dominant over, the short-distance ones. In 2008, the BFs of the radiative charm decays $D^0 \to \bar{K}^{*0}\gamma$ and $D^0 \to \phi\gamma$ were

measured by BABAR to be $(3.22\pm0.20\pm0.27)\times10^{-4}$ and $(2.73 \pm 0.30 \pm 0.26) \times 10^{-5}$, respectively [11], which are consistent with Standard Model predictions [12]. In 2016, Belle reported the observation of $D^0 \to \rho^0\gamma$, $D^0 \to \bar{K}^{*0}\gamma$ and $D^0 \to \phi\gamma$ with BFs of $(1.77 \pm 0.30 \pm 0.07) \times 10^{-4}$, $(4.66\pm0.21\pm0.21)\times10^{-4}$ [13] and $(2.76 \pm 0.19 \pm 0.10) \times 10^{-5}$, respectively. These values are considerably larger than theoretical expectations [14].

To date, however, the radiative decays of charmed baryon Λ_c^+ have rarely been probed in experiment. The bag model, the constituent quark model with QCD corrections and light-cone sum rules predict the BF of the Cabibbo-allowed weak radiative decay $\Lambda_c^+ \to \Sigma^+\gamma$ to be around $10^{-4} - 10^{-5}$ [12, 15, 16]. The decay proceeds predominantly through a W-exchange diagram accompanied by photon emission from the external quark, as shown in Fig. 1. Measurement of the BFs of this kind of decay
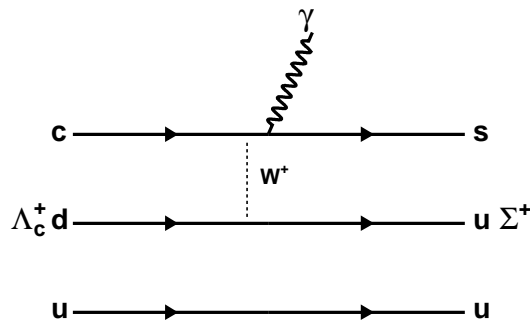

Fig. 1: The lowest-order Feynman diagram of the $\Lambda_c^+ \to \Sigma^+\gamma$ decay.

is important for distinguishing among various theoretical calculations [1, 12, 15, 16], thereby improving the understanding of the weak radiative decay of charmed baryons.

In June 2022, Belle reported the upper limits at 90% credibility level on the absolute branching fraction $\mathcal{B}(\Lambda_c^+ \to \Sigma^+ \gamma) < 2.6 \times 10^{-4}$ [17]. This result is consistent with the theoretical predictions [12, 15, 16]. This paper reports the first search for $\Lambda_c^+ \to \Sigma^+ \gamma$, based on data sample corresponding to an integrated luminosity of 4.5 fb^{-1} accumulated with the BESIII detector at the center-of-mass energies $\sqrt{s} = 4.60 - 4.70$ GeV [18]. The center-of-mass energy and the integrated luminosity for each energy point are listed in Table 1.

Table 1: The center-of-mass energy and the integrated luminosity ($\mathcal{L}_{\text{int}}$) for each energy point. The first and the second uncertainties are statistical and systematic, respectively.

$\sqrt{s}$ (MeV)	$\mathcal{L}_{\text{int}}$ (pb^{-1})
$4599.53 \pm 0.07 \pm 0.74$	$586.90 \pm 0.10 \pm 3.90$
$4611.84 \pm 0.12 \pm 0.28$	$103.45 \pm 0.05 \pm 0.64$
$4628.00 \pm 0.06 \pm 0.31$	$519.93 \pm 0.11 \pm 3.22$
$4640.67 \pm 0.06 \pm 0.36$	$548.15 \pm 0.12 \pm 3.40$
$4661.22 \pm 0.06 \pm 0.29$	$527.55 \pm 0.12 \pm 3.27$
$4681.84 \pm 0.08 \pm 0.29$	$1664.34 \pm 0.21 \pm 10.32$
$4698.57 \pm 0.10 \pm 0.32$	$534.40 \pm 0.12 \pm 3.31$

II. BESIII DETECTOR AND MONTE CARLO

The BESIII detector [19] records symmetric e^+e^- collisions provided by the BEPCII [20] storage ring, which operates in the center-of-mass energy ($\sqrt{s}$) range from 2.0 to 4.95 GeV, with a peak luminosity of 1×10^{33} cm^{-2}s^{-1} achieved at $\sqrt{s} = 3.77$ GeV. BESIII has collected large data samples at these energy regions [21]. The cylindrical core of the BESIII detector covers 93% of the full solid angle and consists of a helium-based multilayer drift chamber (MDC), a plastic scintillator time-of-flight system (TOF), and a CsI(Tl) electromagnetic calorimeter (EMC), which are all enclosed in a superconducting solenoidal magnet providing a 1.0 T magnetic field [22]. The solenoid is supported by an octagonal flux-return yoke with resistive plate counter based muon identification modules interleaved with steel. The charged-particle momentum resolution at 1 GeV/c is 0.5%, and resolution of the ionization energy loss in the MDC (dE/dx) is 6% for electrons from Bhabha scattering. The EMC measures photon energies with a resolution of 2.5% (5%) at 1 GeV in the barrel (end-cap) region. The time resolution in the TOF barrel region is 68 ps, while that in the end-cap region is 110 ps. The end-cap TOF system was upgraded in 2015 using multi-gap resistive plate chamber technology, providing a time resolution of 60 ps [23].

Simulated samples produced with the GEANT4-based [24] Monte Carlo (MC) package, which includes the geometric description [25, 26] of the BESIII detector and the detector response, are used to determine the detection efficiency and to estimate the backgrounds. The simulation includes the beam-energy spread and initial-state radiation (ISR) in the e^+e^- annihilations modeled with the generator KKMC [27]. The inclusive MC sample, which consists of $\Lambda_c^+\bar{\Lambda}_c^-$ events, $D_{(s)}$ production, ISR return to lower-mass ψ states, and continuum processes ($e^+e^- \to u\bar{u}, d\bar{d}$ and $s\bar{s}$) is generated to estimate the potential background, in which all the known decay modes of charmed hadrons and charmonia are modeled with EVTGEN [28, 29] using BFs taken from the Particle Data Group (PDG) [30], and the remaining unknown decays are modeled with LUNDCHARM [31, 32]. Final-state radiation (FSR) from charged final state particles is incorporated using PHOTOS [33]. The $e^+e^- \to \Lambda_c\bar{\Lambda}_c$ lineshape implements the description from [3]. The signal MC events of $\Lambda_c^+ \to \Sigma^+ \gamma$ are modeled with a phase-space generator.

III. METHODOLOGY

At $\sqrt{s} = 4.60 - 4.70$ GeV, $\Lambda_c^+\bar{\Lambda}_c^-$ pairs are produced in e^+e^- annihilations without additional hadrons. The $\bar{\Lambda}_c^-$ baryons are fully reconstructed by their hadronic decays to $\bar{p}K^+\pi^-$, $\bar{p}K_S^0$, $\bar{p}K^+\pi^-\pi^0$, $\bar{p}K_S^0\pi^0$, $\bar{p}K_S^0\pi^+\pi^-$, $\bar{\Lambda}\pi^-$, $\bar{\Lambda}\pi^-\pi^-\pi^+$, $\bar{\Lambda}\pi^-\pi^0$, $\bar{\Sigma}^0\pi^-$ and $\bar{\Sigma}^-\pi^+\pi^-$. These reconstructed decays are referred to as single-tag (ST) $\bar{\Lambda}_c^-$ baryons, where the intermediate particles K_S^0, $\bar{\Lambda}$, $\bar{\Sigma}^0$, $\bar{\Sigma}^-$, and π^0 are reconstructed via $K_S^0 \to \pi^+\pi^-$, $\bar{\Lambda} \to \bar{p}\pi^+$, $\bar{\Sigma}^0 \to \gamma\bar{\Lambda}$, $\bar{\Sigma}^- \to \bar{p}\pi^0$ and $\pi^0 \to \gamma\gamma$, respectively. In the other side of the events recoiling against the ST $\bar{\Lambda}_c^-$ baryons, the candidate $\Lambda_c^+ \to \Sigma^+ \gamma$ decays are selected to form double-tag events (DT).

IV. ST EVENT SELECTION

The same selection criteria are used in this analysis as in Ref. [10]. Charged tracks are required to have a polar angle (θ) within $|\cos\theta| < 0.93$, where θ is defined with respect to the beam direction. Except for those from K_S^0 and $\bar{\Lambda}$ decays, all tracks are required to originate from an interaction region defined by $|V_{xy}| < 1$ cm and $|V_z| < 10$ cm, where $|V_{xy}|$ and $|V_z|$ refer to the distances of closest approach of the reconstructed track to the interaction point (IP) in the xy plane and the z direction (along the beam), respectively.

Particle identification (PID) is implemented by combining the measurements of dE/dx in the MDC and the flight time in the TOF into a probability that a given track is a pion, kaon or proton. The track is assigned to one of these three particle types, according to the probability.

Candidates for K_S^0 and $\bar{\Lambda}$ mesons are reconstructed from their decays to $\pi^+\pi^-$ and $\bar{p}\pi^+$, respectively, where the charged tracks must have distances of closest approach to the IP that are within ± 20 cm along the

beam direction. To improve the signal purity, PID is implemented to select the antiproton candidate, while the charged pion is not subject to any PID requirement. A secondary vertex fit is performed for each K_S^0 or $\bar{\Lambda}$ candidate, and the momenta updated by the fit are used in the subsequent analysis. The K_S^0 or $\bar{\Lambda}$ candidate is accepted if the χ^2 of the secondary vertex fit is less than 100. Furthermore, the decay vertex is required to be separated from the IP by a distance of at least twice the fitted vertex resolution, and the invariant mass to be within $(0.487, 0.511)\,\mathrm{GeV}/c^2$ for $\pi^+\pi^-$ or $(1.111, 1.121)\,\mathrm{GeV}/c^2$ for the $\bar{p}\pi^+$ pair. The two invariant mass for $\pi^+\pi^-$ and $\bar{p}\pi^-$ resolutions are found, using MC simulations, to be 2.9 MeV/c^2 and 1.2 MeV/c^2, respectively. The $\bar{\Sigma}^0$ and $\bar{\Sigma}^-$ candidates are reconstructed from the $\gamma\bar{\Lambda}$ and $\bar{p}\pi^0$ final states with invariant masses being within (1.179, 1.203) GeV/c^2 and (1.176, 1.200) GeV/c^2, respectively. The two invariant mass resolutions are found, using simulation, to be 3.6 MeV/c^2 and 4.3 MeV/c^2, respectively.

Photon candidates are identified using showers in the electromagnetic calorimeter (EMC). The deposited energy of each shower must be more than 25 MeV in the barrel region ($|\cos\theta| \leq 0.80$) or more than 50 MeV in the end-cap region ($0.86 \leq |\cos\theta| \leq 0.92$). To suppress electronic noise and showers unrelated to the event, the difference between the EMC time and the event start time is required to be within [0, 700] ns.

The π^0 candidates are reconstructed with pairs of photon candidates within the invariant mass range (0.115, 0.150) GeV/c^2. To improve the resolution, a kinematic fit is performed by constraining the invariant mass of the photon pair to correspond to the π^0 mass and requiring the corresponding χ^2 of the fit to be less than 200. The momenta updated by the kinematic fit are used in the subsequent analysis.

To distinguish the ST $\bar{\Lambda}_c^-$ baryons from combinatorial backgrounds, we study the distributions of the energy difference ΔE and the beam-constrained mass M_{BC} of the selected ST candidates, defined as

$$\Delta E \equiv E_{\bar{\Lambda}_c^-} - E_{\mathrm{beam}}, \qquad (1)$$

$$M_{\mathrm{BC}} \equiv \sqrt{E_{\mathrm{beam}}^2/c^4 - |\vec{p}_{\bar{\Lambda}_c^-}|^2/c^2}, \qquad (2)$$

where E_{beam} is the beam energy, and $\vec{p}_{\bar{\Lambda}_c^-}$ and $E_{\bar{\Lambda}_c^-}$ are the total momentum and energy of the ST candidate, respectively, calculated in the e^+e^- rest frame. The signals are expected to concentrate around zero in ΔE distribution and around the nominal $\bar{\Lambda}_c^-$ mass in the M_{BC} distribution. If there are multiple candidates for each tag mode, the one with minimum $|\Delta E|$ is retained. Combinatorial backgrounds in the M_{BC} distributions are suppressed with the ΔE requirements shown in Table 2.

For each tag mode, the ST yield is determined by fitting the M_{BC} distribution of the candidates accepted by all the requirements described. In the fit, the $\bar{\Lambda}_c^-$ signal is modeled with a shape obtained from the MC-simulated

signal convolved with Gaussian function, different for different energies and tagging modes, and the combinatorial background is described by an ARGUS function [34]. The fits to the M_{BC} distributions for the various tag modes at $\sqrt{s} = 4.600\,\mathrm{GeV}$ are shown in Fig. 2. Candidates in the M_{BC} signal region, $(2.275, 2.310)\,\mathrm{GeV}/c^2$, are kept for further analysis. The ST yields in data and the ST efficiencies for individual tags are shown in Table 2. The same procedure is performed for the other six data samples at different energy points which are summarized in the Supplementary materials of Ref. [10]. Summing over the ST yields for all tags and energy points gives the total ST yield to be $N_{\mathrm{ST}}^{\mathrm{tot}} = 105244 \pm 384$, where the uncertainty is statistical.
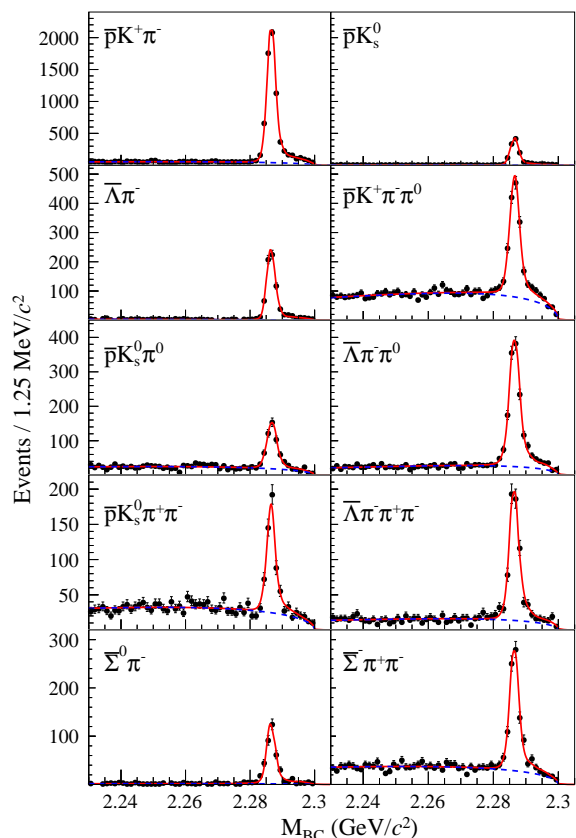

Fig. 2: Distributions of M_{BC} for the different ST channels of the $\bar{\Lambda}_c^-$ at $\sqrt{s} = 4.600$ GeV. The signal shape of the $\bar{\Lambda}_c^-$ is described by the simulated shape convolved with a Gaussian resolution function and the background is modeled with an ARGUS function. The points with error bars represent data. The (red) solid curves indicate the fit results and the (blue) dashed curves describe the background shapes.

V. DT EVENT SELECTION

After the selection of the tag side, the $\Lambda_c^+ \rightarrow \Sigma^+\gamma$ ($\Sigma^+ \rightarrow p\pi^0$) is selected in the recoil side of the tagged $\bar{\Lambda}_c^-$

Table 2: The ΔE requirement, ST yield, and ST detection efficiency (include the branching fractions of subleading decays) of $\bar{\Lambda}_c^- \to \bar{\Sigma}^- \gamma$ for each tag mode for the data sample at $\sqrt{s} = 4.600$ GeV. The uncertainty in the ST yield is statistical only.

Tag mode	ΔE(MeV)	N_i^{ST}	ϵ_i^{ST}(%)
$\bar{p}K^+\pi^-$	$(-34,\ 20)$	6705 ± 90	51.0
$\bar{p}K_S$	$(-20,\ 20)$	1268 ± 37	56.2
$\bar{\Lambda}\pi^-$	$(-20,\ 20)$	741 ± 28	47.7
$\bar{p}K^+\pi^-\pi^0$	$(-30,\ 20)$	1539 ± 57	15.4
$\bar{p}K_S\pi^0$	$(-30,\ 20)$	485 ± 29	18.4
$\bar{\Lambda}\pi^-\pi^0$	$(-30,\ 20)$	1382 ± 49	16.6
$\bar{p}K_S\pi^+\pi^-$	$(-20,\ 20)$	512 ± 29	19.9
$\bar{\Lambda}\pi^-\pi^+\pi^-$	$(-20,\ 20)$	646 ± 31	13.7
$\bar{\Sigma}^0\pi^-$	$(-20,\ 20)$	404 ± 22	22.5
$\bar{\Sigma}^-\pi^+\pi^-$	$(-30,\ 20)$	872 ± 38	18.1

Table 3: The DT detection efficiency (include the branching fractions of subleading decays) in percent for each tag mode and each energy point.

$\sqrt{s}$ (GeV)	4.600	4.612	4.628	4.641	4.661	4.682	4.699
$pK^-\pi^+$	12.9	12.7	12.2	11.9	11.6	11.2	10.9
pK_S^0	13.8	13.2	12.7	12.0	11.6	11.2	11.0
$\Lambda\pi^+$	10.4	10.0	9.6	9.1	8.8	8.7	8.0
$pK^-\pi^+\pi^0$	4.4	4.3	4.1	3.9	3.8	3.8	3.6
$pK_S^0\pi^0$	4.7	4.6	4.4	4.2	4.1	4.0	3.9
$\Lambda\pi^+\pi^0$	4.1	3.7	3.7	3.7	3.4	3.5	3.3
$pK_S^0\pi^+\pi^-$	5.2	4.8	4.6	4.7	4.4	4.3	4.1
$\Lambda\pi^+\pi^+\pi^-$	3.6	3.4	3.3	3.1	3.2	3.1	3.1
$\Sigma^0\pi^+$	6.0	5.5	5.1	5.4	4.8	4.8	4.8
$\Sigma^+\pi^+\pi^-$	4.7	4.3	4.3	4.2	4.3	3.9	3.9

as follows. It is required to have only one good charged track identified as a proton, apart from those charged tracks used in the ST selection. The proton candidate is required to originate from within 20 cm along the beam axis with respect to the IP. The π^0 candidates are selected with photon pairs, and the energies of the photons are required to be less than 0.45 GeV, which is a requirement set from the study of the $\pi^0 \to \gamma\gamma$ distribution in signal MC at generator level. The energy of the radiative isolated high energy γ is required to be greater than 0.65 GeV, and the number of good photons must be exactly one for the signal process. For multiple π^0 candidates, only the combination of the proton, π^0 and radiative γ with minimum of $|\Delta E_{\mathrm{sig}}|$ is retained, where $\Delta E_{\mathrm{sig}} = E_{p\pi^0\gamma} - E_{\mathrm{beam}}$. The ΔE_{sig} is further required to be within $(-0.038, 0.026)$ GeV. The Σ^+ candidate is reconstructed via $\Sigma^+ \to p\pi^0$ with a mass $(M_{p\pi^0})$ lying within $(1.176, 1.200)$ GeV/c^2.

To determine the detection efficiency, 500,000 events of $\Lambda_c^+ \to \Sigma^+\gamma$ are simulated for each energy point. The ten tag modes are simulated according to their relative BFs. The DT efficiencies measured from this MC sample are summarized in Table 3 after all selection requirements.

VI. BACKGROUND ANALYSIS

Potential sources of background are classified into two categories: those directly originating from continuum hadron production in e^+e^- annihilation (denoted as $q\bar{q}$ background thereafter) and those from $e^+e^- \to \Lambda_c^+\bar{\Lambda}_c^-$ (denoted as $\Lambda_c^+\bar{\Lambda}_c^-$ background thereafter).

The $M_{\mathrm{BC}}^{\mathrm{sig}}$ distribution of the accepted candidates from the $q\bar{q}$ component in the inclusive MC sample is shown in Fig. 3(a), where no peaking contribution in the signal region is observed. The yield of the $q\bar{q}$ component in the signal region $M_{\mathrm{BC}}^{\mathrm{sig}} \in (2.275, 2.310)$ GeV/c^2 is estimated from the data to be 5.0 ± 0.2 events, which is determined by measuring the number of data events in the sideband

region $M_{\mathrm{BC}}^{\mathrm{sideband}} \in (2.15, 2.27)$ GeV/c^2. The $M_{\mathrm{BC}}^{\mathrm{sig}}$ distributions in the inclusive MC sample show that the background components are consistent between sideband and signal regions. This sideband contribution has been extrapolated to the signal region with a scale factor 1.03, which is the ratio between sideband region and signal region in the inclusive MC sample.

The $\Lambda_c^+\bar{\Lambda}_c^-$ background is dominated by events containing the decay $\Lambda_c^+ \to \Sigma^+\pi^0$, the magnitude of which is estimated using MC simulation. The expected background yield from this source is estimated in MC simulation and found to be 6.2 ± 0.5 events after normalizing to the integrated luminosity of the data sample and taking $\mathcal{B}(\Lambda_c^+ \to \Sigma^+\pi^0) = (1.24 \pm 0.10) \times 10^{-2}$ from the PDG [30]. The resulting M_{BC} distribution of the accepted candidates in data, signal MC and various simulated background contributions is presented in Fig. 3(a), where the signal MC is shown with a BF $= 1.0 \times 10^{-4}$, which corresponds to an event yield of 1.2 events. There are 10 events in data in the signal region.

VII. UPPER LIMIT CALCULATION

Since no significant signal is observed, a test statistic based on a profile log-likelihood ratio [35] is used to determine the upper limit on the BF of $\Lambda_c^+ \to \Sigma^+\gamma$. The likelihood function depending on the parameter of interest $\mathcal{B}(\Lambda_c^+ \to \Sigma^+\gamma)$ and the nuisance parameters $\theta_1 = (\epsilon_{\mathrm{eff}}, N_{\mathrm{bkg}})$ is defined as

$$\mathcal{L}(\mathcal{B}(\Lambda_c^+ \to \Sigma^+\gamma), \theta_1) = \mathrm{Pois}(N_{\mathrm{obs}}|N_{\mathrm{exp}}) \cdot \mathrm{Gaus}(\theta_1), \quad (3)$$

where Pois is a Poisson function, Gaus is a Gaussian distribution, N_{obs} is the number of events observed in the signal region from data. N_{exp} is the expected number of events, which is defined as the sum of the number of background and signal events estimated in the signal region,

$$N_{\mathrm{exp}} = 2N_{\Lambda_c^+ \bar{\Lambda}_c^-} \cdot \mathcal{B}_{\mathrm{ST}} \cdot \mathcal{B}(\Lambda_c^+ \to \Sigma^+ \gamma) \cdot \epsilon_{\mathrm{eff}} + N_{\mathrm{bkg}}, \quad (4)$$

where $N_{\Lambda_c^+ \bar{\Lambda}_c^-}$ is the number of $N_{\Lambda_c^+ \bar{\Lambda}_c^-}$ pairs, $\mathcal{B}_{\mathrm{ST}}$ stands for the BF of a given tag mode, ϵ_{eff} refers to signal efficiency and N_{bkg} is the number of background events. The systematic uncertainties are parameterized as Gaussian-function constraints with nuisance parameters θ_1. The uncertainties associated with the efficiency and background are considered separately. The upper limit on the BF at a confidence level (CL) of 90% is derived by scanning the parameter of interest space, with result shown in Fig. 3(b), and is found to be $\mathcal{B}(\Lambda_c^+ \to \Sigma^+ \gamma) < 4.4 \times 10^{-4}$.

VIII. SYSTEMATIC UNCERTAINTIES

With the DT method, most of the systematic uncertainties arising from the ST side cancel out. However, systematic uncertainties originate from other sources. The uncertainty in the total ST yield is assigned as 0.5% [28], which comes mainly from the statistical uncertainty, with an additional systematic component associated with the fit to the M_{BC} distribution of the ST candidates, assessed by varying the signal shape, the background shape, and the fit range in the fit to the M_{BC} distributions. The uncertainties due to the proton tracking and PID efficiencies are studied with a control sample of reconstructed $J/\psi \to p\bar{p}\pi^+\pi^-$ process. These are assigned to be 2.0% and 1.0%, respectively. The uncertainties associated with the difference in π^0 reconstruction efficiencies between data and MC simulation are estimated using DT events with $\bar{D}^0 \to K^+\pi^-$, $K^+\pi^-\pi^-\pi^+$ versus $D^0 \to K^-\pi^+\pi^0$. The systematic uncertainty in the reconstruction efficiency per radiative photon is based on the studies with the control sample of $J/\psi \to \rho^0\pi^0$ with $\rho^0 \to \pi^+\pi^-$ and $\pi^0 \to \gamma\gamma$ [36] and is assigned to 1.0%. The difference of π^0 efficiencies between data and MC simulation, 1.0%, is assigned as the associated systematic uncertainty [37]. The uncertainty due to the requirement on only one proton candidate is estimated from a sample of $J/\psi \to \Sigma^0\bar{\Sigma}^0$ ($\Sigma^0 \to p^+\pi^-$) decays. The efficiency difference between this requirement and the nominal one is 2.0%, which is assigned as a systematic uncertainty. The potential bias due to the $M_{p\pi^0}$ requirement is estimated with the $J/\psi \to \Sigma^+\Sigma^-$ sample, with the 0.4% difference of efficiencies between data and simulation being assigned as the corresponding uncertainty. The systematic uncertainty due to the ΔE_{sig} requirement is estimated in a similar manner with the $\Lambda_c \to p\pi^0\pi^0$ sample and found to be 3.1%. The potential bias associated with the $q\bar{q} \to$ hadrons background contribution is assigned from the the statistical uncertainty of the data
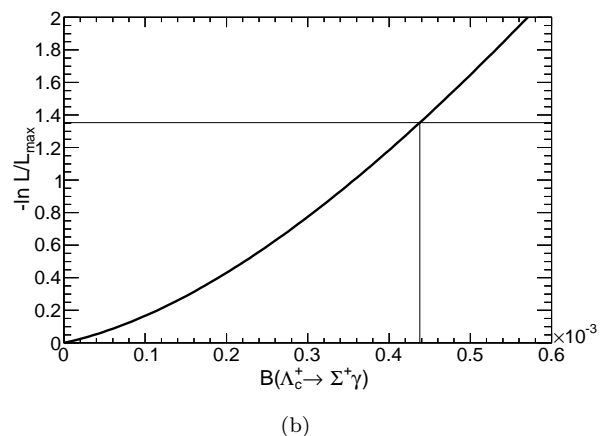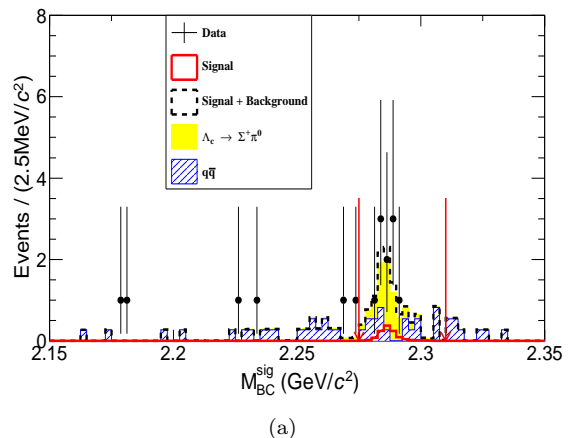

(a)

(b)

Fig. 3: (a) The comparison of the $M_{\mathrm{BC}}^{\mathrm{sig}}$ distributions of the candidate events for $\Lambda_c^+ \to \Sigma^+\gamma$ between data and MC simulation. The two red arrows indicate the signal region. (b) The profile log-likelihood ratio curve versus $\mathcal{B}(\Lambda_c^+ \to \Sigma^+\gamma)$. The intersection of the curve and horizontal line indicates the upper limit of the BF at the 90% CL, where the black solid curve is the scan result with systematic uncertainties.

yield in the sideband range of the $M_{\mathrm{BC}}^{\mathrm{sig}}$ distribution (2.15, 2.27) GeV/c^2, which is used to estimate this background, and leads to a 4.4% uncertainty in the branching fraction. The total systematic uncertainty from the $q\bar{q} \to$ hadrons background contamination is assigned to be 2.1% as the quadratic sum of the above two sources. The systematic uncertainty associated with the $\Lambda_c \to \Sigma\pi^0$ background contribution is 4.4% based on the knowledge of the BF from PDG [30]. To study the effects of the uncertainty in the MC model we generate the $\Lambda_c^+ \to \Sigma^+\gamma$ events with a proton polar-angle distribution parameterized by $1 + \alpha\cos^2\theta$ (with $\alpha = \pm 1.0$), and find a difference of 2.1% in efficiency with respect to the baseline phase-space model. The limited size of the signal MC sample leads to a 0.6% uncertainty in the knowledge of the efficiency. Table 4 summarizes the sources of the systematic uncertainties in the measurement of branching ratio of $\Lambda_c^+ \to \Sigma^+\gamma$ de-

cay. The total systematic uncertainty is obtained to be 7.3% as the quadratic sum of all sources.

Table 4: Summary of relative systematic uncertainties (in %).

Sources	$\mathcal{B}(\Lambda_c^+ \to \Sigma^+\gamma)$ (%)
Single-tag yield	0.5
p tracking	2.0
p PID	1.0
γ detection	1.0
π^0 reconstruction	1.0
N_{proton} requirement	2.0
Signal model	2.1
Σ^+ requirement	0.4
ΔE requirement	3.1
$q\bar{q}$ background	2.1
$\Lambda_c \to \Sigma\pi^0$ background	4.4
Assumed BF (PDG)	0.6
MC statistics	0.6
Sum	7.3

IX.   SUMMARY

Using an e^+e^- collision data sample corresponding to an integrated luminosity of 4.5 fb^{-1} collected at $\sqrt{s} = 4.60 - 4.70$ GeV with the BESIII detector, we have searched for the Cabibbo-allowed weak radiative decay $\Lambda_c^+ \to \Sigma^+\gamma$ for the first time. No signal is found, and an upper limit on the BF of $\Lambda_c^+ \to \Sigma^+\gamma$ decay is set to be 4.4×10^{-4} at the 90% CL. This result is consistent with the theoretical predictions of 5×10^{-5} [12], 2.8×10^{-4} [15] and 1.03×10^{-4} [16], from the Bag model and appropriate QCD corrections, respectively, where the short-distance $cd \to us\gamma$ mechanism is expected to be dominant. A more stringent constraint, or discovery, is expected with the larger data set that BESIII expects to accumulate in the near future [39].

[1] H. Y. Cheng, Front. Phys. (Beijing), 101406 (2015).

[2] H. Y. Cheng, Chin. J. Phys. **78** 324-362 (2022).

[3] M. Ablikim *et al.* (BESIII Collaboration), Phys. Rev. Lett. **120**, 132001 (2018).

[4] M. Ablikim *et al.* (BESIII Collaboration), Phys. Rev. Lett. **116**, 052001 (2016).

[5] M. Ablikim *et al.* (BESIII Collaboration), Phys. Rev. D **95**, 111102 (2017).

[6] M. Ablikim *et al.* (BESIII Collaboration), arXiv:2207.14149.

[7] M. Ablikim *et al.* (BESIII Collaboration), Phys. Rev. Lett. **117**, 232002 (2016); Phys. Rev. Lett. **120**, 029903 (2018).

[8] A. Zupanc *et al.* (Belle Collaboration), Phys. Rev. Lett.

113, 042002 (2014).

[9] Aaij, R *et al.* (LHCb Collaboration), Phys. Rev.D 97, 091101 (2018).

[10] M. Ablikim *et al.* (BESIII Collaboration), Phys. Rev. Lett. **128**, 142001 (2022).

[11] B. Aubert *et al.* (BABAR Collaboration), Phys. Rev. D **78**, 071101 (2008).

[12] H. Y. Cheng *et al.*, Phys. Rev. D **51**, 1199 (1995).

[13] A. Zupanc *et al.* (Belle Collaboration), Phys. Rev. Lett. **118**, 051801 (2017).

[14] A. Khodjamirian, G. Stoll, and D. Wyler, Phys. Lett. B **358**, 129 (1995).

[15] T. Uppal and R.C. Verma Phys. Rev. D **47**, 2858 (1993).

[16] Shi, Yu-Ji and Xing, Zhi-Peng and Meißner, Ulf-G., arXiv:2212.01111.

[17] A. Zupanc *et al.* (Belle Collaboration), arXiv:2206.12517.

[18] M. Ablikim *et al.* (BESIII Collaboration), arXiv:2203.03133.

[19] M. Ablikim *et al.* (BESIII Collaboration), Nucl. Instr. Method A **614**, 345 (2010).

[20] C. H. Yu *et al.*, Proceedings of IPAC2016, Busan, Korea (JACoW, Geneva, Switzerland, 2016).

[21] M. Ablikim *et al.* (BESIII Collaboration), Chin. Phys. C **44**, 040001 (2020).

[22] K.X. Huang *et al.*, Nucl. Sci. Tech. **33**, 142 (2022).

[23] X. Li *et al.*, Radiat. Detect. Technol. Methods **1**, 13 (2017); Y. X. Guo *et al.*, Radiat. Detect. Technol. Methods **1**, 15 (2017)

[24] S. Agostinelli *et al.* (GEANT4 Collaboration),Nucl. Instrum. Meth. A **506**, 250 (2003).

[25] Y. Liang, B. Zhu, and Z. Y. You *et al.*, Nucl. Instrum. Meth. A **603**, 325 (2009).

[26] Z. Y. You, Y. T. Liang, and Y. J. Mao, Chin. Phys. C **32**, 572 (2008).

[27] S. Jadach, B. F. L. Ward, and Z. Was, Phys. Rev. D **63**, 113009 (2001); Comput. Phys. Commun. **130**, 260 (2000).

[28] D. J. Lange, Nucl. Instrum. Meth. A **462**, 152 (2001).

[29] R. G. Ping, Chin. Phys. C **32**, 599 (2008).

[30] P.A. Zyla *et al.* (Particle Data Group),Prog. Theor. Exp. Phys. **2020**, 083C01 (2020) and 2021 update.

[31] J. C. Chen, G. S. Huang, X. R. Qi, D. H. Zhang, and Y. S. Zhu, Phys. Rev. D **62**, 034003 (2000).

[32] R. L. Yang, R. G. Ping, and H. Chen, Chin. Phys. Lett. **31**, 061301 (2014).

[33] E. Richter-Was, Phys. Lett. B **303**, 163 (1993).

[34] H. Albrecht *et al.* (ARGUS Collaboration), Phys. Lett. B **241**, 278 (1990).

[35] G. Cowan, K. Cranmer, E. Gross and O. Vitells, Eur. Phys. J. C **71**, 1554 (2011).

[36] M. Ablikim *et al.* (BESIII Collaboration), Phys. Rev. D **96**, 051101 (2017).

[37] M. Ablikim *et al.* (BESIII Collaboration), Phys. Rev. D **103**, 112007 (2021).

[38] M. Ablikim *et al.* (BESIII Collaboration), Phys. Rev. D **674**, 100, 072004 (2019).

[39] M. Ablikim *et al.* (BESIII Collaboration), Chin. Phys. C **44**, 040001 (2020).